Correlation between Structure and Vapor Sorption in Semicrystalline Linear Polyethylene: One Dimensional Nano-Swelling Measured Using in Situ Vapor Sorption Small Angle Neutron Scattering (iVSANS)

Man-Ho Kim*

Materials Science and Technology Research Division, Korea Institute of Science and Technology (KIST) PO BOX 131, Seoul 130-650, Korea

Charles J. Glinka

NIST Center for Neutron Research, National Institute of Standards and Technology, Gaithersburg, Maryland 20899-6102

Received October 22, 2008; Revised Manuscript Received February 7, 2009

ABSTRACT: Changes in the nanoscale structure of semicrystalline polyethylene (PE) resulting from the sorption/diffusion of hexane-d_{14} vapor have been observed and quantified by *in situ* vapor sorption small-angle neutron scattering (iVSANS). We find a linear correlation between vapor sorption/diffusion and nanoexpansion of the amorphous phase within the lamellae confined in the spherulite domains. The expansion depends on the degree of crystallinity and spherulite perfection. We measured the structure-based sorption kinetics and isotherms of samples with two different crystalline volume fractions (ϕ_{vc}). The low crystalline polyethylene shows a larger expansion in the long period, L, than the high crystalline polyethylene. Low crystalline PE shows a Fickian-like diffusion profile with sorption time while the high crystalline PE ($\phi_{vc} = 78\%$) shows a S-shape diffusion profile (non-Fickian) at $P/P^\circ = 0.95$. The diffusion coefficient increases with relative vapor pressure (P/P°) in both materials. The apparent diffusion coefficient in the low crystalline polymer is approximately a factor of 2 higher than that of the more crystalline polymer. On the other hand, effective diffusion coefficients, D_{eff}'s, normalized with the amorphous volume fractions at each vapor activity are identical regardless of crystallinity. This indicates that amorphous volume fraction is the predominant factor that controls transport properties, at least for small diffusing molecules. Furthermore, the one-dimensional expansion is reversible during cyclic sorption and desorption processes, suggesting that the crystals were not destroyed unlike the inference of a previous study.[1]

Introduction

Linear polyethylene (PE), one of the most common polymers, has the simplest composition, consisting only of carbon and hydrogen, $-(CH_2-CH_2)_n-$, and molecular structure, consisting only of a repeating unit of the covalently bonded carbon with a bonding angle of 112° and a carbon−carbon bond distance of 1.54 Å in the molten state.[2] Despite the simple structures, PE is semicrystalline, consisting of either two phases, amorphous and crystalline phase, or three phases, in the case of the existence of an interfacial region between the two phases. The structure and morphology of this semicrystalline polymer have been extensively studied. Yet there have been relatively few studies aimed at correlating nanoscale structural changes with sorption and diffusion of solvents.[3] Most sorption and diffusion studies have used a standard gravimetric method[4−6] in addition to infrared spectroscopy.[7,8] Diffusion and sorption is important in the areas of barrier materials,[9,10] biomaterials,[11] polyelctrolyte-like fuel cell membranes,[12] gas or vapor separation, and gas-phase polymerization of polyolefins.[13] We recently used the iVSANS technique to verify the commonly held assumption that solvent vapor selectively diffuses into the amorphous regions of semicrystalline polymers.[3,14−16] The diffusion occurs through both the amorphous phase in the lamellae (at nanometer scale along the thickness direction and at micrometer scale along the lateral dimension) and that in the grain boundary between spherulites (at micrometer scale). The iVSANS technique and the selective penetration of vapor into the amorphous phase allow us to trace nanostructural change in the amorphous phase between the crystalline lamellae and between the spherulites. The purpose of this study is to systematically investigate correlations between the structure of lamellae geometrically confined in spherulite and the sorption and diffusion behavior of small molecules in semicrystalline materials.

* Corresponding author. E-mail: man-hokim@kist.kr.

Experimental Section

Linear polyethylene (weight averaged molar mass $M_w = 101.3$ kg/mol with polydispersity of around 1.9) was crystallized in two ways. Both samples were initially melted at 443 K for around 10 min, 28 K above the equilibrium melting temperature ($T_m^o = 415.2$ K) of linear polyethylene with $M_w \sim 101$ kg/mol,[17] to remove any traces of crystalline nuclei. A high crystalline sample ($\phi_{vc} = 78\%$, PE78) was isothermally crystallized at the preset temperature ($T_c = 383.0 \pm 0.5$ K) for 36 h. A low crystalline sample ($\phi_{vc} = 54\%$, PE54) was rapidly crystallized at $T_c = 296.0$ K by quenching the melt in water. The former has a low supercooling, ($\Delta T = T_m^o - T_c$), of 32.2 K, compared with 119.2 K for the latter. The volume crystallinity, ϕ_{vc}, was estimated from density measurements using a density gradient column with a methanol/ethylene glycol mixture at 296 K. Density was converted to crystalline volume fraction with the relation $\phi_{vc} = (\rho - \rho_a)/(\rho_c - \rho_a)$, where ρ, ρ_a (=0.85 g/cm^3), and ρ_c (=1.00 g/cm^3) are the densities of sample, ideal amorphous phase, and orthorhombic unit cell, respectively. The samples were 0.10 ± 0.01 mm thick. Additional sample preparation details are given in ref 3.

Details on the iVSANS scattering apparatus, principles of operations, and apparatus performance are described elsewhere.[18] With this equipment relative vapor pressure of degassed hexane-d_{14} was dynamically controlled by monitoring the absolute vapor pressure in the *in situ* vapor sorption cell, feeding and removing

10.1021/ma802363d CCC: $40.75
Published on Web 03/13/2009

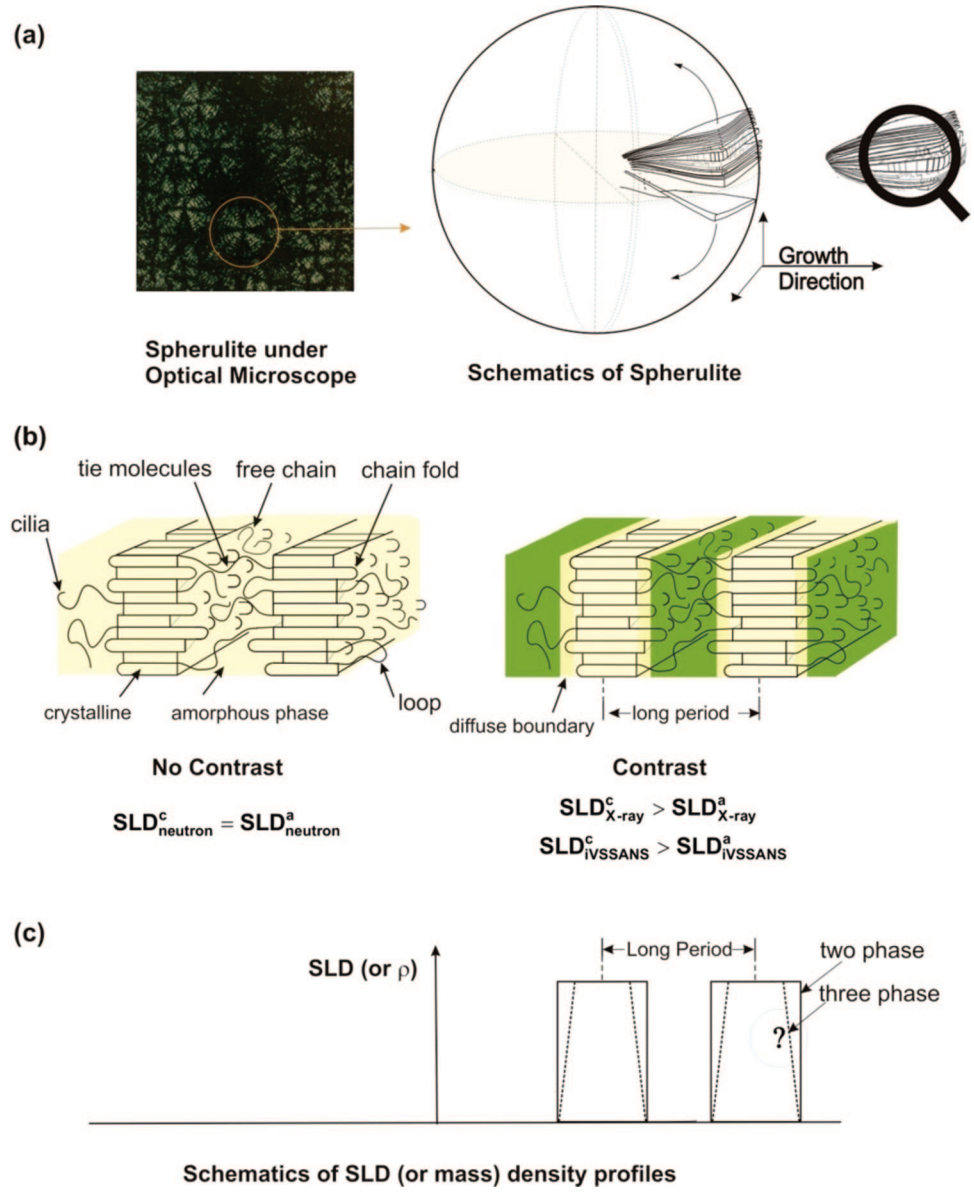

Figure 1. (a) Schematics of spherulite, (b) lamellar stacks confined in spherulite, and (c) scattering length density between amorphous and crystalline phases in the lamellae.The green color indicates the contrast (i.e., electron density difference between twophases) of dry amorphous phase against crystalline phase for X-ray or the contrast(i.e., difference in neutron scattering length) between the sorbed contrast generating vapor (and/or liquid) for iVSANS. SLD stands for scattering length density. Parts b and c) were modified from Figure 1 of ref 3.

vapor whenever the pressure in the cell deviated from a target vapor pressure. Relative vapor pressure is expressed as $P/P°$, where P and $P°$ stand for partial and saturation vapor pressures at a given temperature, respectively. A SANS measurement was started immediately after the target pressure was reached. The iVSANS experiment was performed on the NG3 30-m SANS instrument at the NIST Center for Neutron Research. The sample-to-detector distance was 10.55 m with an wavelength $\lambda = 5.5$ Å and a relative wavelength spread $\Delta\lambda/\lambda \approx 14.3\%$. The transmission of dry PE78 and PE54 was about 93 and 91%, respectively. Additional ultra small angle neutron scattering (USANS) measurements, to cover approximately two decades lower ($q \sim 3 \times 10^{-5}$Å^{-1}) than the low q limit of the NG-3 SANS instrument, were done on a dedicated Bonse−Hart-type diffractometer,[19] BT5, at the NCNR. For the USANS measurements the samples were removed from the sorption cell, wet with liquid hexane-d_{14} and confined between two quartz windows. After measurement, no indication of evaporation was observed. Measuring SANS and USANS together allows us to investigate a broad range of structure from nanometers to micrometers. The SANS and USANS data were reduced to an absolute scale (cross section per unit volume) with the data reduction package provided at the NCNR.[20]

Results

SANS from dry PE does not show strong scattering while SAXS does (Figure 1 of ref 3). The former is due to the near cancelation, $b_c + 2b_H \approx 0$, of neutron scattering lengths between the carbon ($b_C = 6.646$ fm) and two hydrogens ($2b_H = -7.478$ fm) in the monomer unit. This causes weak neutron contrast between the crystalline and amorphous phases despite the mass density difference between the two phases in the dry polymers (Figure 1b). The negligible neutron contrast can be overcome by sorbing a small amount of contrast generating vapor, provided the vapor goes selectively into one phase (i.e., amorphous phase) (Figure 1b). Experimental verification of such selective sorption was reported in ref 3.

As vapor (for example, hexane-d_{14} for polyolefins) penetrates selectively into the amorphous phase (green color in Figure 1b), neutron scattering cross-section increases due to the enhance-

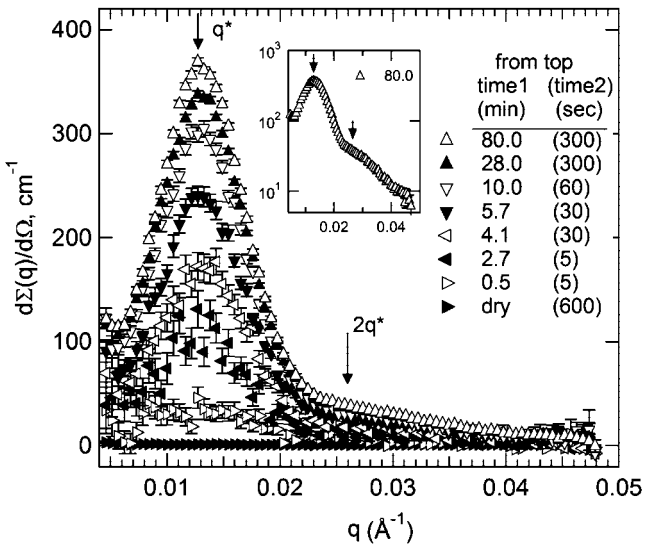

Figure 2. iVSANS profiles measured at the indicated sorption time (time 1)$P/P^\circ = 0.95$ at for PE78. Time2 is the counting time (s) of each iVSANS measurement. Inset is a semilog plot showing the second reflection, $2q^*$.

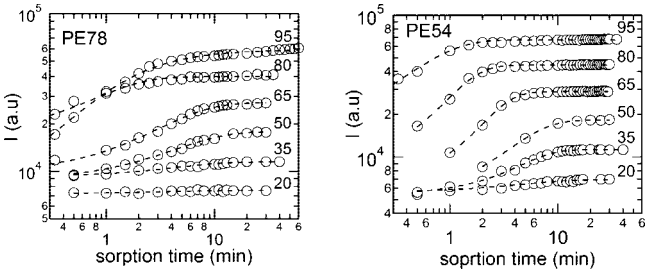

Figure 3. Intensity vs sorption time of PE54 and PE78. Intensity is the total detector counts recorded in 5 min. The scattered intensity increases then levels off after about 10 min at each relative vapor pressure.

ment of neutron contrast between crystalline and amorphous/hexane-d_{14} phases. Figure 2 clearly demonstrates that the coherent scattering cross-section (i.e., absolute intensity) is negligible for dry polyethylene and increases with sorption time at a fixed relative vapor pressure of 95%. Orderly growth of the cross-section with sorption time allows us to study diffusion/sorption kinetics from the iVSANS measurements. Unlike conventional gravimetric methods, the sorption measurement from iVSANS is not affected by the amount of sorbent on the surface of the sample films because the total scattering cross-section is enhanced only when the vapor selectively penetrates into one (i.e, amorphous phase in semicrystalline polymers) of the phases. Thus, the measurement truly reflects sorption in the bulk of the material as well as the amorphous phase of lamellae. The profiles at other P/P° values are similar to Figure 2 except for the total cross-section and peak position that depend on the amount of sorbed vapor.

With a series of measurements at other relative vapor pressures ($P/P^\circ = 80$, 65, 50, 35, and 20%), we can plot the kinetics as shown in Figure 3.

Figure 4a shows the profiles of PE54 equilibrated at the indicated P/P° during stepwise sorption and desorption. The entire profile including the peak around $q = 0.022$ Å^{-1} grows with vapor pressure preserving the profile shape. The two-dimensional scattering images, Figure 4b, show the corresponding distribution of the scattering as color contour plots. The isotropic contour (doughnut) shape does not change during the cyclic sorption and desorption, which suggests that the isotropic distribution of lamellae remains unchanged. Figure 4c shows the quick response time of the apparatus to reach and maintain the target pressure.

Discussion

The Bragg peak in Figures 2 and 4 directly gives the long period ($L=2\pi/q^*$, q^* is the peak position) that represents the spacing between amorphous (or crystalline) layers in the lamellar stacks within the spherulite regions of the samples. Lamellar structure was confirmed with the second reflection ($2q^* \sim 0.025$ Å^{-1}) of PE74 as shown in the inset (semilog plot) of Figure 2. SAXS also shows the lamellar structure for both PE78 and PE54.[3] The values of long period are plotted in Figures 5 and 6.

Figure 5 shows the change of the long period with sorption time. The long period increases sigmoidally with the time. The equilibrium values of L are plotted versus relative vapor pressure in Figure 6. The long period increases linearly with vapor pressure. The increase of L is mainly due to the linear expansion of amorphous phase since the vapor does not penetrate the crystalline phase.[3] The average thickness of the crystalline region in the lamellae before sorption $\langle l_c \rangle$ ($=L_o\phi_{vc}$) is $263.8 \times 0.54 = 142.5$ Å and $470.6 \times 0.78 = 367.1$ Å for dry PE54 and PE78, respectively, where the long spacing L_o of the dry polymer was obtained from the extrapolation to $P/P^\circ = 0$. As expected, the thickness of the lamellae of PE78 is greater than that of PE54. We can relate this observation to the two crystallization processes, the initial lamellar formation process during primary crystallization and the lamellar thickening process during secondary crystallization. Initial lamellar thickness is inversely proportional to the supercooling ($l^* \propto c/\Delta T$, c is a thermodynamic parameter during the primary crystallization).[21−23] Lamellar thickness further increases with crystallization time during the secondary crystallization. PE78 has a lower supercooling ($\Delta T = 32.2$ K) and a longer crystallization time compared with PE54 so that the lamellar thickness of PE78 becomes larger than that of the quenched PE54. We note also that the change of long spacing with relative vapor pressure (dL/da, with $a = P/P^\circ$) for PE54 (=0.30) is steeper than that (=0.14) of PE78.

The average thickness, $\langle l_a \rangle$, of the amorphous layers in the lamellae was obtained as follows: since the crystalline thickness is constant (i.e., $\langle l_c \rangle_{dry} = \langle l_c \rangle_{wet} = \langle l_c \rangle$), regardless of wetting or drying, due to the impermeability of vapor into the crystalline phase,[3] the average thickness of the amorphous layer, $\langle l_a \rangle$ during wetting can be estimated from $\langle l_a(t,a) \rangle = L(t,a) - \langle l_c \rangle$. For dry PE54 and PE78, the values of $\langle l_a \rangle$ are 121.3 and 103.5 Å, respectively. Hence it is the amorphous layer thickness that increases linearly with increasing relative vapor pressure [Figure 6].

The average amorphous lamellar layer thickness $\langle l_a \rangle$ of the low crystallinity PE54 is larger than that of the high crystallinity PE78. One-dimensional swelling, $\delta l_a = \langle l_a \rangle - l_a^0$, increases linearly up to about 30 Å (25 ± 2%) for PE54 and 14 Å (14 ± 1%) for PE78 in the full range (0−1.0) of P/P° (or 12 and 7 Å from 0.2 to 0.95 in the measured range). This means that the low crystalline PE54 absorbed more vapor than the highly crystalline PE78. Since PE54 is the rapidly crystallized sample, spherulites have less time to develop and the distribution of lamellar thicknesses becomes broad. This results in larger scattering peak widths, as shown in Figure 8. On the other hand, since PE78 was isothermally crystallized at low supercooling for a relatively long time (approximately 1.5 days), spherulites become well developed, with a narrower distribution of lamellar thicknesses and higher packing density of crystalline lamellae compared to PE54. Spherulites of PE78 are expected to cause a severe geometrical constraint against the expansion of amorphous phase. Taut tie molecules that bridge the neighboring

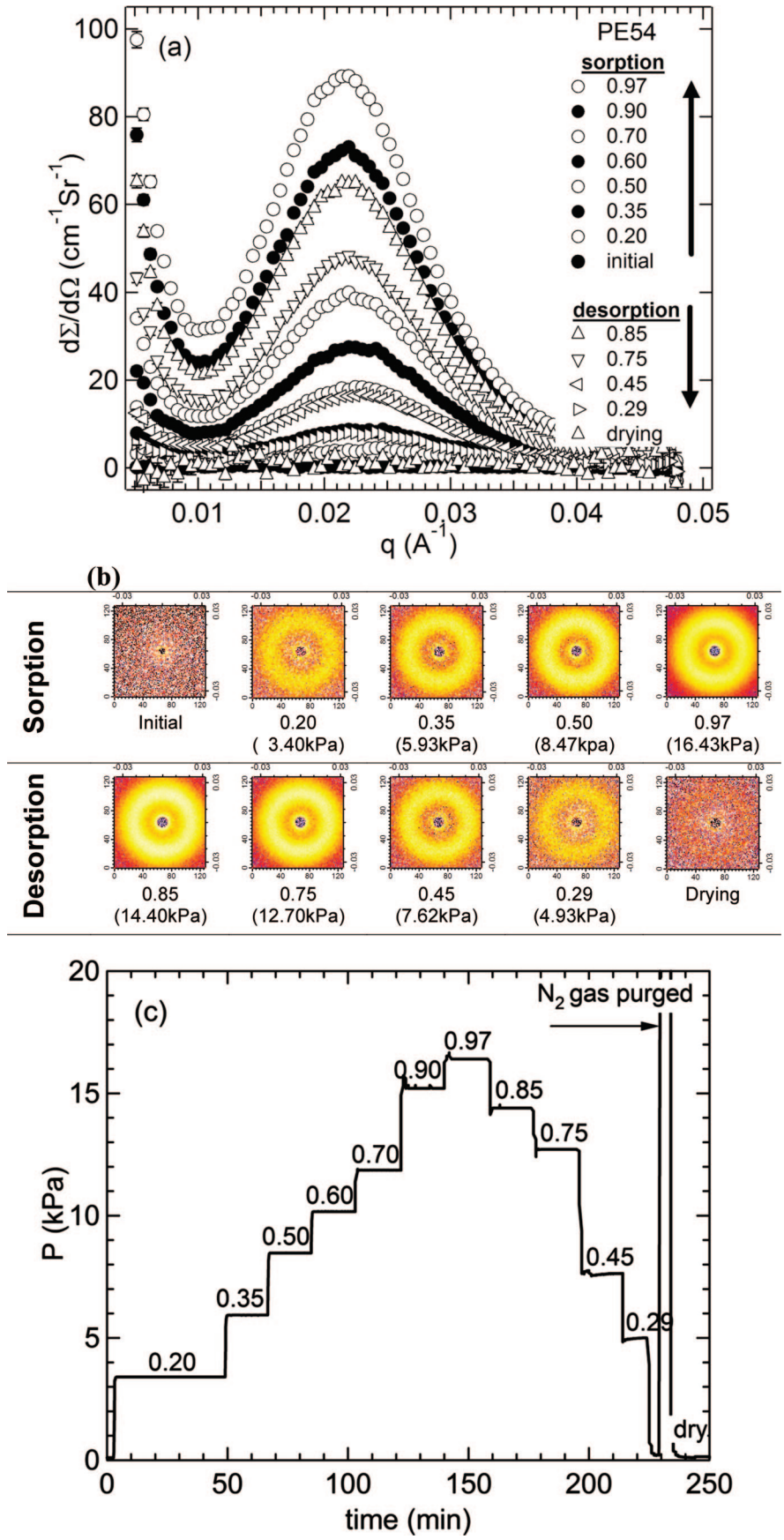

Figure 4. iVSANS profiles (a) of PE54 equilibrated at the indicated P/P^o during stepwise sorption (circle) and desorption (triangle) (a), and corresponding 2D scattering images (b). The response time to reach a target pressure and the stability at that pressure is shown in part c. All measurements (run time ~ approximately 15 min) were performed at a temperature of 21.0 ± 0.1 °C. *n*-Hexane, P^o(21 °C) = 16.94 kPa, rather than hexane-d_{14} was used for the response-time measurements. Following the measurements, the sample was purged with flowing dry nitrogen gas and dried under vacuum.

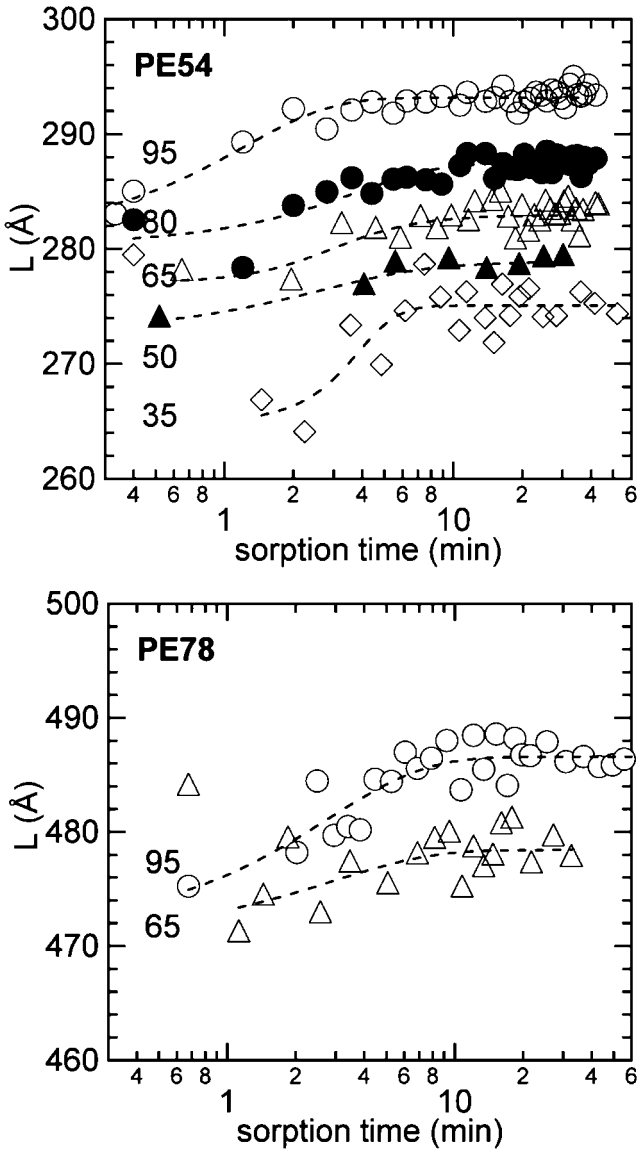

Figure 5. Long period (L) vs sorption time at the indicated relative vapor pressure (%).

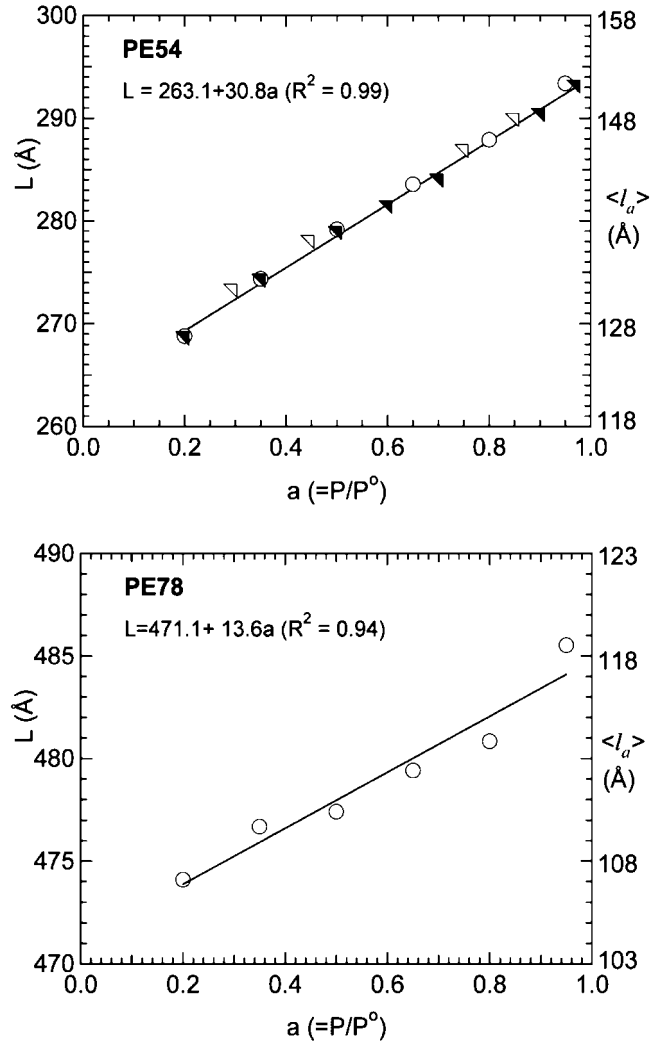

Figure 6. Long spacing versus relative vapor pressure of hexane-d_{14}. The measurement of L was conducted at the equilibrium condition at each relative vapor pressure. Measurements were repeated, varying the approach to equilibrium, to demonstrate reproducibility. The symbols, ○ (all sorption kinetics measured starting from dry membrane), ▲ (from sorption after jumping from the next R/P° after the measurement), △ equilibrium at desorption).

crystalline layers can be another reason that limits the swelling in nanoscale. The population of tie molecules in linear polyethylene is estimated to be less than 1%.[24] Such a small fraction of tie molecules likely has minimal effect on the swelling behavior. Other possible molecular parameters such as cilia, free chains, loose loop, and loose tie molecules in the amorphous phase play a role to increase free volume, which would enhance the sorption and swelling. In the well-defined spherulite, therefore, the reduced swelling is likely due to the geometrical constraint rather than the tie molecules.

It is of interest to know whether the crystals are stable during sorption/desorption process. If the crystals were dissolved or disrupted by vapor, the long period would change. The reversibility of L and $\langle l_a \rangle$ during the cyclic sorption and desorption process (as shown in PE54 of Figure 6) indicates that vapor does not destroy the crystalline lamellae in semicrystalline polyethylene, which differs from the inference discussed in other work.[1,25] The reversibility [memory effect in some sense] in the long period is due to the elasticity of the amorphous phase confined in the lamellae.

The total detector count rates at equilibrium (the plateau count rates in Figure 3, for example) at each relative vapor pressure during sorption and desorption are plotted in Figure 7 for PE54. This plot is effectively the absorption/desorption isotherm for the sample. The data in Figure 7 show reversibility with vapor activity during sorption and desorption. The reversibility is a further indication that the underlying nanoscale structure is not altered by the absorption/desorption of the hexane vapor.

The full width at half-maximum (fwhm) of the peak in the small angle scattering is related to the size distribution of lamellar spacings. The fwhm of PE54 is broader than that of PE78 [see Figure 8], indicating the former has a broader size distribution of lamellae. At higher vapor activity and longer sorption time, the fwhm becomes slightly narrower in both PE54 and PE78. At a very low vapor content, the broad distribution of interlamellar distances seems to slightly rearrange to form a narrower distribution at higher vapor content.

So far we have discussed the correlation between sorption and structure. Of interest is to investigate whether the nature of the amorphous phase affects the diffusion behavior of vapor.

The typical diffusion plot for Fickian second law, the reduced intensity against the square root of sorption time, is shown in Figure 9.[26] Details of the data treatment for this plot using iVSANS measurement is given in ref 12. PE54 [Figure 9 a] shows typical Fickian diffusion behavior within our experimental

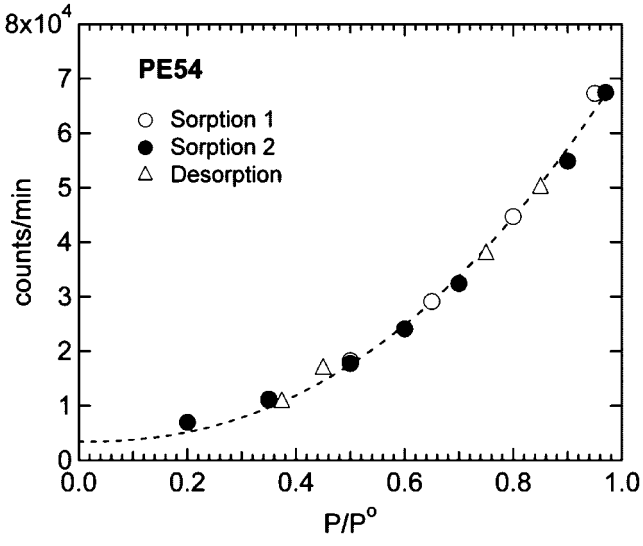

Figure 7. Sorption and desorption isotherm, as measured by the total detector count rate, of PE54. Soprtion 1 was measured from the level off of Figure 3. Sorption 2 and desorption were measured in a stepwise manner as shown in Figure 4c.

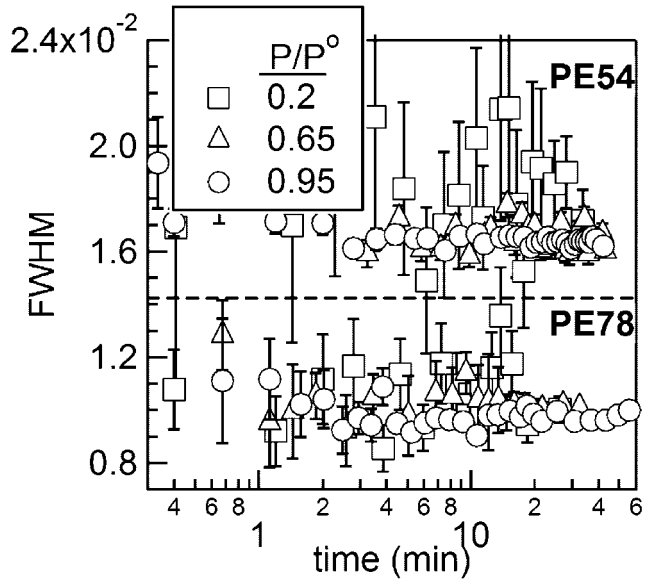

Figure 8. Fwhm of the peak in the scattering of the rapidly crystallized PE54 and isothermally crystallized PE78. The broken line is drawn to distinguish the fwhm between PE54 and PE78. Fwhm was determined from the Lorentzian fit. Error bars represent ± σ.

error range while PE78 (Figure 9 b) shows a S-shape sorption profile (i.e., non-Fickian diffusion), especially at high relative vapor pressure. These results are identical with Rogers' gravimetric measurement for linear polyethylene measured at 0 °C.[25] Rogers explained the S-shape sorption profile (time dependent diffusion) as due to some rearrangement or relaxation of polymer structure during the early stage of sorption. If we accept the relaxation concept, the densely packed amorphous chain of PE78 could have a slower relaxation time than the low crystalline PE54.

The penetrant, *n*-hexane, and amount of sorption increase the free volume in semicrystalline polyethylene during sorption.[27−29] Molecular packing of amorphous phase for the high crystalline PE78 is expected to be tight (i.e., less free volume) at this stage, which hinders the penetration of vapor and is evidenced with a shallow slope. As vapor continuously sorbs to a site for sorption, the sorbed vapor may play a role as a plasticizer and increase

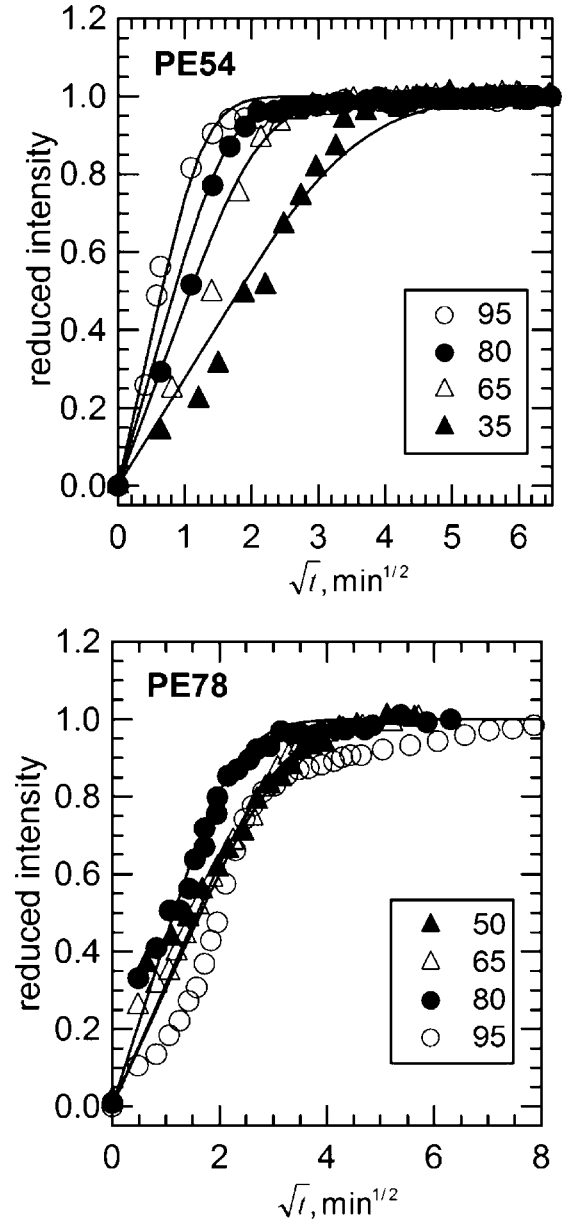

Figure 9. Fickian second law Diffusion plot of PE54 and PE78 at the indicated *P*/*P*°. The solid line is calculated with Fick's second law.

the free volume so that the amount of sorption increases as indicated with a steep slope.

Different chain packing in the confined amorphous phase can be further investigated with a diffusion coefficient. Diffusion coefficient (D, cm^2/min) was determined from the initial slope in the plot (Figure 9) of the reduced total intensity versus the square root of the sorption time, $\sqrt{t}$, based on Fick's second law; (D = slope × sample thickness × $\sqrt{\pi}$ /4)^2.[12] Figure 10a shows that PE54 has roughly a factor of 2 higher diffusion coefficients than PE74 at the same vapor activity. Large free volume (i.e., open space) and amorphous fraction of PE 54 could provide more space for the vapor to diffuse into the loosely packed lamellae while the tight chain packing of PE78 restricts the penetration of vapor. Thus, the former has the higher diffusion coefficient. Crystallinity has been known to affect sorption and diffusion.[30−33] The diffusion coefficient can be further normalized with an amorphous fraction $\phi_a(t,a)$.

$$D_{\text{eff}}\,(\text{cm}^2/\text{min}) = D/\varphi_a(t,a) \qquad (1)$$

The amorphous content at each activity ($a = P/P^\circ$) was estimated from the long period $L(t\rightarrow\infty,a)$ and amorphous thickness $l_a(t\rightarrow\infty,a)$ at equilibrium condition ($t\rightarrow\infty$):

$$\varphi_a(t,a) = \frac{l_a(t \rightarrow \infty, a)}{L(t \rightarrow \infty, a)} \quad (2)$$

assuming that the dimensional change along the lateral dimension of the amorphous layer can be neglected because the lateral dimension is so large compared to the amorphous thickness. Figure 10b shows the effective diffusion coefficient (D_{eff}) with vapor activity. The D_{eff}'s of the PE54 and PE78 superimpose each other keeping the linear increase with vapor activity. This demonstrates that amorphous fraction, with its free volume, is the predominant factor that controls transport properties. Studies show that both chain conformation (tie molecules, entanglement, et al.) restricted in the amorphous phase of lamellae and the stresses imposed on the phase can be other factors that affect the transport properties, depending on the size of penetrant and magnitude of the elastic stress.[30−32] Since a systematic study on the size of diffusants has not been done in this study, at least we may say that the D_{eff} of *n*-hexane vapor in the semicrystalline polyethylene does not show any difference in the nature of amorphous phase. One possible reason is that the size of *n*-hexane is not large enough to distinguish the subtle

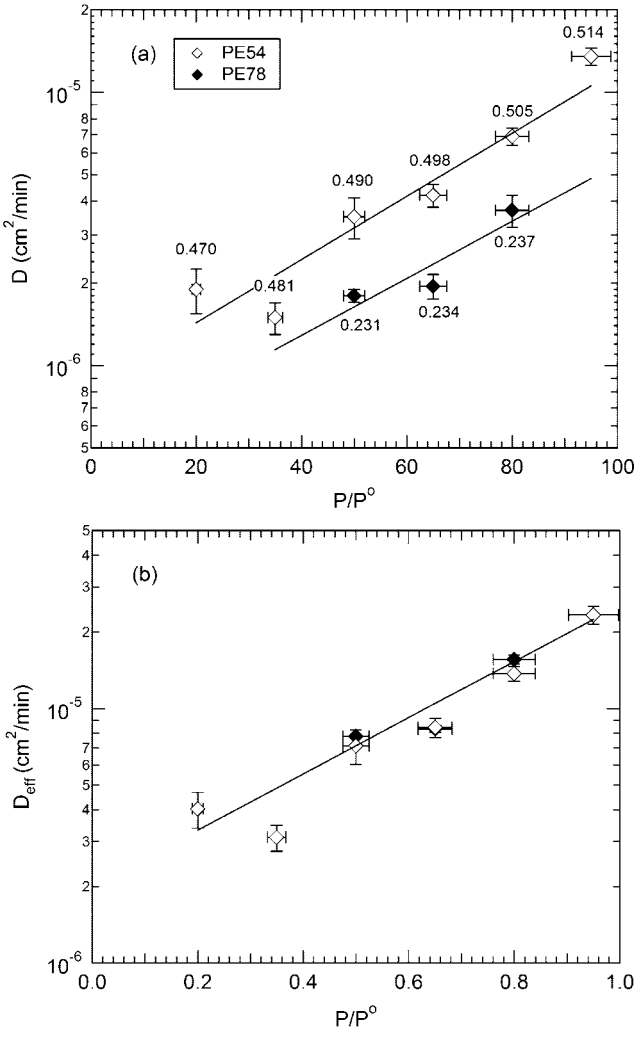

Figure 10. (a) Diffusion coefficient of PE54 (open) and PE 78 (closed) at 21 °C and the indicated amorphous fractions, $\phi_a(t,a)$. (b) Effective diffusion coefficient, D_{eff}, normalized with amorphous volume fraction.

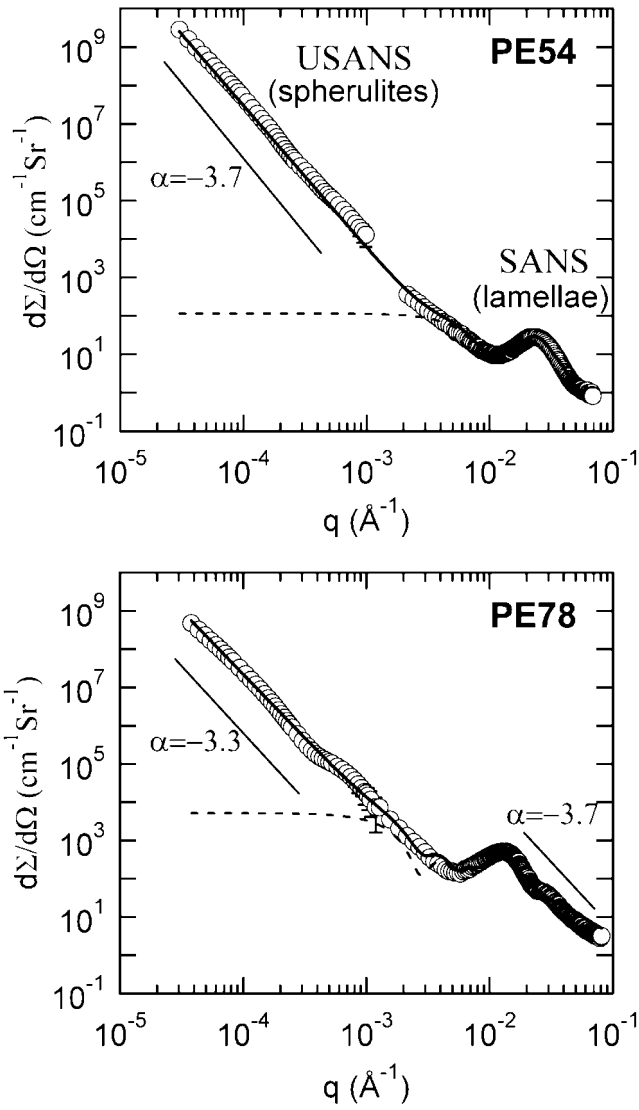

Figure 11. USANS and SANS of the PE54 and PE78 samples saturated with hexane-d_{14} solvent. The solid line was calculated from the paracrystalline model[30] with a Gaussian distribution function for lamellae (dotted) plus the fractal scattering in USANS region. For PE54, the average crystalline $\langle l_c\rangle \pm \sigma_c$ and amorphous thickness $\langle l_a\rangle \pm \sigma_a$ of the lamellae are about 115 ± 16 and 121 ± 59 Å, respectively, with an average number of lamellae per stack of $\langle N\rangle = 2.5$. The power law exponent in the low q region is about −3.7. For PE78, $\langle l_c\rangle \pm \sigma_c$ and $\langle l_a\rangle \pm \sigma_a$ are 246 ± 97 Å and 194 ± 58 Å, respectively. $\langle N\rangle = 5$. Detail changes in the slope of the USANS region are neglected on fitting.

nature (chain conformation, elastic stress, packing, et al.) of the amorphous phase geometrically confined in spherulite.

A strong upturn in the scattering was observed below $q = 0.01$ Å^{-1} (Figure 4) and it is necessary to investigate the low q region further. USANS measurements for the vapor saturated PE54 and PE78 show that the low q upturn extended down to $q = 3.0 \times 10^{-5}$ Å^{-1}. This low angle scattering is indicative of a broad distribution of spherulite sizes, averaging over 10 μm in diameter. This was confirmed with an optical microscope [Figure 1]. The low q scattering in the range of q from 10^{-5} to 10^{-3} Å^{-1} shows a power law scattering defined as $I(q) \approx q^{-\alpha}$. The scattering exponent α is defined as $\alpha = 2d - D_s$ for surface fractal with the limit of $d < 2d - D_s < d + 1$ or $\alpha = D_m$ for mass fractal with the limit of $1 < D_m < 3$, where d is the dimension of an object.[34] The $\alpha \approx 3.7$ for PE54 and $\alpha \approx 3.3$ for PE78 in Figure 11 correspond to surface fractal dimensions of $D_s \approx 2.3$ and $D_s \approx 2.7$, respectively. This may indicate that

the spherulite surface becomes rough on isothermally crystallizing at high temperature. The power law scattering above $q \approx 0.02$ Å^{-1}, the region of lamellae structure, shows $\alpha \approx 3.7$ for PE78. On the other hand, PE54 does not extend far enough in q range for any meaningful quantitative analysis. Fractal analysis of this region is shown in the literature.[35]

Conclusions

Our analysis of the kinetics of hexane vapor absorption/desorption in two samples of semicrystalline PE with widely different crystalline volume fractions, PE54 ($\phi_{vc} = 0.54$) and PE78 ($\phi_{vc} = 0.78$), has given new insight into their microstructure and its relationship to absorptive capacity and diffusion rates. We have specifically found that the amorphous layers in the spherulite domains of PE54 increase in thickness by a larger percentage (~25%) than those of PE78 (~14%) at saturated vapor pressure of *n*-hexane at room temperature, indicating that the amorphous layers are more constrained in the more crystalline sample (PE78). The nanostructural change in the amorphous phase is reversible during sorption and desorption cycle and the structure of the crystalline phases is stable. Nevertheless, the rate at which hexane molecules diffuse through the amorphous regions of both samples, as evidenced by their diffusion constants (D_{eff}) normalized by amorphous volume fraction is essentially the same. This might be that the nature of amorphous phase in both low and high crystalline polyethylene is likely the same or that the size of *n*-hexane molecule is not large enough to distinguish the subtle difference in both samples. These results are relevant both to processing methods for tailoring the barrier and sorptive properties of semicrystalline polymer films and to theoretical work on the transport behavior of semicrystalline polymers.

Acknowledgment. This paper is dedicated to the memory of R. O. Lawton Distinguished Professor Leo Mandelkern, who was a leading and talented scholar in polymer physics, especially in phase transformation of polymers. This work utilized facilities supported in part by the National Science Foundation under Agreement No. DMR-0454672. M.H.K. acknowledges support by the KIST (2E20844). We thank B. Hammouda for reviewing the manuscript and reviewers for comments.

References and Notes

(1) Rogers, C. E.; Stannett, V.; Szwarc, M. *J. Phys. Chem.* **1959**, *63*, 1406–1413.
(2) Kim, M.-H.; Londono, J. D.; Habenschuss, A. *J. Polym. Sci., B: Polym. Phys.* **2000**, *38*, 2480–2485.
(3) Kim, M.-H.; Glinka, C. J. *J. Appl. Crystallogr.* **2005**, *32*, 734–739.
(4) Mandelkern, L.; Long, F. A. *J. Polym. Sci.* **1951**, *51*, 457–469.
(5) *Diffusion in Polymer*; Crank, J., Park, G. S., Eds.; Academic Press: London and New York, 1968.
(6) Robens, E.; Rubner, K.; Staszczuk, P. *J. Therm. Anal. Cal.* **2004**, *76*, 639–646.
(7) Lane, R. A.; Buckton, G. *Int. J. Pharm.* **2000**, *207*, 49–56.
(8) Duarte, A. R.; Anderson, L. E.; Duarte, C. M. M.; Kazarian, S. G. *J. Supercrit. Fluids* **2005**, *36*, 160–165.
(9) Kale, G.; Kijchavengkul, T.; Auras, R.; Rubino, M.; Selke, S. E.; Singh, S. P. *Macromol. Biosci.* **2007**, *7*, 255–277.
(10) *Barrier Polymers and Structures,* ; Koros W. J., Ed.; ACS Symposium Series 423; American Chemical Society: Washington, DC, 1990.
(11) Ito, S.; Hashimoto, M.; Wadgaonkar, B.; Svizero, N.; Carvalho, R. M.; Yiu, C.; Rueggeberg, F. A.; Foulger, S.; Saito, T.; Nishitani, Y.; Yoshiyama, M.; Tay, F. R.; Pashley, D. H. *Biomaterials* **2005**, *26*, 6449–6459.
(12) Kim, M.-H.; Glinka, C. J.; Grot, S. A.; Grot, W. A. *Macromolecules* **2006**, *39*, 4775–4787.
(13) Novak, A.; Bobak, M.; Kosek, J.; Banaszak, B. J.; Lo, D.; Widya, T.; Ray, W. H.; de Pablo, J. J. *J. Appl. Polym. Sci.* **2006**, *100*, 1124–1136.
(14) Moore, S.; Wanke, S. *Chem. Eng. Sci.* **2001**, *56*, 4121–4129.
(15) Hutchinson, R.; Ray, W. *J. Appl. Polym. Sci.* **1990**, *41*, 51–81.
(16) Bonavoglia, B.; Storti, G.; Morbidelli, M.; Rajendran, A.; Mazzotti, M. *J. Polym. Sci., B: Polym. Phys.* **2006**, *44*, 1531–1546.
(17) Kim, M.-H.; Phillips, P. J.; Lin, J. S. *J. Polym. Sci., Part B: Polym. Phys.* **2000**, *38*, 154–170.
(18) Kim, M.-H.; Glinka, C. J.; Carter, R. N. *Rev. Sci. Instrum.* **2005**, *76*, 113904–10.
(19) Barker, J. G.; Glinka, C. J.; Moyer, J. J.; Kim, M.-H.; Drews, A. R.; Agamalian, M. *J. Appl. Crystallogr.* **2005**, *38*, 1004–1011.
(20) Kline, S. R. *J. Appl. Crystallogr.* **2006**, *39*, 895–900.
(21) Hoffman, J. D.; Lauritzen, J. I. *J. Res. NBS* **1960**, *64A*, 73–102.
(22) Hoffman, J. D.; Miller, R. L. *Polymer* **1997**, *38*, 3151–3212.
(23) Keller, A. *Pure Appl. Chem.* **1992**, *64*, 193–204.
(24) Huang, Y.-L.; Brown, N. *J. Polym Sci., Part B: Polym. Phys.* **1991**, *29*, 129–137.
(25) Rogers, C. E.; Stannett, V.; Szwarc, M. *J. Polym. Sci.* **1960**, *45*, 61–82.
(26) Crank, J. *The Mathematics of Diffusion*, 2nd ed.; Oxford University Press: New York 1975.
(27) Liu, C.-P. A.; Neogi, P. *J. Membr. Sci.* **1988**, *35*, 207–215.
(28) Ng, H. C.; Leung, W. P.; Choy, C. L. *J. Polym. Sci. Polym. Phys.* **1985**, *23*, 973–989.
(29) Peterlin, A. *Polym. Eng. Sci.* **1977**, *17*, 183–193.
(30) Klein, J.; Briscol, B. J. *Nature* **1977**, *266*, 43–44.
(31) Michaels, A. S.; Bixler, H. J.; Fein, H. L. *J. Appl. Phys.* **1964**, *35*, 3165–3178.
(32) Michaels, A. S.; Hausslein, R. W. *J. Polym. Sci. C* **1965**, *10*, 61–86.
(33) Eby, R. K. *J. Appl. Phys.* **1964**, *35*, 2720–2724.
(34) Martin, J. E.; Hurd, A. J. *J. Appl. Crystallogr.* **1987**, *20*, 61–78.
(35) Ogawa, T.; Miyashita, S.; Miyaji, H.; Suehiro, S.; Hayashi, H. J. *J. Chem. Phys.* **1989**, *90*, 2063–2067.

MA802363D